Numerical simulations of dense clouds on steep slopes: Application to powder-snow avalanches

by Jocelyn Étienne, Pierre Saramito
Laboratoire de Modélisation et Calcul, IMAG, Grenoble
and Emil J. Hopfinger
Laboratoire des Écoulements Géophysiques et Industriels, HMG, Grenoble

Preprint to the Annals of Glaciology, vol. 38

Abstract

In this paper two-dimensional Direct Numerical Simulations (DNS) of dense clouds moving down steep slopes are presented for the first time. The results obtained are in good agreement with the overall characteristics – that is, the spatial growth rate and velocity variations – of clouds studied in the laboratory. Direct numerical simulations give, in addition to the overall flow structure, local density and velocity variations inside the cloud, not easily accessible in experiments. The validity of two-dimensional simulations as a first approach is justified by the dynamics of the flow and by comparison with experimental results. The interest of the results for powder-snow avalanches is discussed, concluding that two-dimensionality is acceptable and that large density differences need to be taken into account in future simulations.

Introduction

A powder-snow avalanche is a dense cloud of suspended snow particles moving down a steep slope. These flows can reach front velocities u_f of 100 m s^{-1}, and heights h of the order of 100 m. Measurements by intrusive probes are, therefore, very hazardous. In addition, powder-snow avalanches are rare events. Techniques such as georeferenced photography and radar now in use provide extremely valuable information concerning the avalanche dimensions, their shape and front velocities as well as velocities behind the front (Dufour and others, 2000, 2001). However, density or snow concentration measurements still rely on intrusive probes and are relatively uncertain.

In parallel, laboratory experiments, simulating avalanches, were developed which gave useful information about the dynamics of these flows and the dependency of avalanche velocity and shape on slope angle. A review of laboratory experiments and the related theoretical models can be found in Hopfinger (1983) and Hutter (1996). The theoretical models show that entrainment of snow from the snow cover is an important aspect of avalanche motion (Hopfinger and Tochon-Danguy, 1977; Fukushima and Parker, 1990; Rastello and Hopfinger, in press). Generally, laboratory experiments are, unfortunately, limited to Boussinesq fluids of Boussinesq number $\frac{\varrho_2-\varrho_1}{\varrho_2} \ll 1$. The principle similarity parameter is the densimetric Froude number provided the Reynolds number is sufficiently large for the flow to be fully turbulent (in free shear flows a continuous energy spectrum with a $k^{-\frac{5}{3}}$ spectral slope emerges when the flow Reynolds number is greater than $3 \cdot 10^4$).

Commercial avalanche codes use depth averaged models and in some cases turbulence k-ε models for the powder cloud. Often these models are combined with a dense flow layer below the powder cloud and a transition layer in between (see e.g. Naaim and Gurer, 1998).

In order to make progress in the understanding of the flow structure, more refined experiments are required (field studies and laboratory experiments). Direct Numerical Simulations (DNS) and Large Eddy Simulations (LES) are alternative approaches. These give access to all the flow quantities desired and would be of particular interest for the study of the interaction of an avalanche with structures for instance. Unfortunately, the complex structure of avalanches make such numerical simulations still difficult. For this reason only Boussinesq gravity currents on horizontal boundary have been simulated at present (Necker and others, 2002). Here we present the first DNS of dense clouds motion on slopes. These simulations are, at present, two-dimensional and for $\frac{\varrho_2-\varrho_1}{\varrho_2} \ll 1$; the relevance of 2D simulations which allow to reach high Reynolds numbers, is supported by the dynamics of avalanches discussed below. Before refining the simulations by going to a 3D code, it is of interest to study first such first order effects as snow entrainment and large $\frac{\varrho_2-\varrho_1}{\varrho_2}$. Ultimately, DNS and LES can serve as bench mark tests for averaged models used in practice.

Characteristics and dynamics of powder-snow avalanche flow

The density of avalanches ranges from about 20 kg m^{-3} near the start to about 2 kg m^{-3} at the end. The settling velocity and volume concentration of the snow particles are small, so that the energy required to keep the particles in suspension is a small fraction of the turbulent kinetic energy. Furthermore, the particle time scale $\tau_p = \frac{w_s}{g}$ (where w_s is the fall velocity and g the gravitational acceleration) is about one tenth of the flow time scale $\frac{h}{u_f}$ Hence, the particles follow closely the local velocity of the cloud, which allows, as a first approximation, to treat the avalanche as a variable density fluid.

Laboratory experiments with dense clouds carried out by Beghin and others (1981), Hermann and others (1987) and more recently by Rastello (2002) showed that the main features of avalanche flow can be reproduced with single-phase, variable-density flows, and demonstrated two essential features of these flows:

- The force balance governing the flow is between the driving buoyancy force and the entrainment of ambient fluid (air in the case of avalanches). As ambient fluid is entrained it has to be accelerated, and this momentum transfer results in an effective drag, which has an effect of a much larger magnitude than ground friction. There is practically no flow separation, so that the form drag is negligible. The interfacial friction is included in the entrainment.
- The entrainment of ambient fluid is caused by the overturning motion of the large structures of the flow.

The generation of the large structures, responsible for the entrainment of ambient fluid, is essentially a two-dimensional mechanism. The smaller-scale three-dimensional turbulence of the flow is superimposed on the larger features. The effect of these three-dimensional structures on the air entrainment can be neglected in a first-order approach. Indeed, Normand (1990) demonstrated by comparison with numerous laboratory experiments that two-dimensional simulations of a mixing layer reproduce closely the actual spreading rate of the flow. Therefore, we can expect that two-dimensional direct numerical simulations can fairly closely reproduce the essential physics and dynamics of laboratory clouds and also powder-snow avalanches. This allows us to focus on solving accurately this simplified problem rather than dealing with the complexity of three-dimensional simulations.

Within this frame, we shall proceed first with validating our assumptions by comparing the simulations with laboratory clouds, for which we have accurate quantitative results. Then the simulations are extended to avalanches.

The comparison with laboratory experiments allows two further approximations which will provisionally be used in our simulations: (i) The ratio of the density of the aerosol to the ambient fluid density is close to one (whereas it is closer to 10 for avalanches), i.e. we can use the Boussinesq approximation ; (ii) the Reynolds number is of order 10^4, rather than 10^9 for avalanches. It should be noted that the actual value of the Reynolds number is not of primary importance (because the dynamics is controlled by the large-scale features and depends only weakly on the smaller scales) as long as it is sufficiently large ($\mathrm{Re} \geq 10^4$).

Small scale laboratory dense clouds are limiting cases of avalanches, as was clearly shown by Rastello by comparing laboratory results with observations by Dufour and others (2001).

Variable-density flow equations

Let us consider a fluid which is a mixture of two miscible species with different properties, and define a volume fraction of each of them, Φ_1 and Φ_2, in a domain Ω, such that $\Phi_1 + \Phi_2 = 1$. In our case, the species are the initial dense fluid (snow aerosol) and the ambient fluid (air).

Following Joseph and Renardy (1993), we assume that the diffusion within the mixture is governed by Fick's law, and assuming Boussinesq conditions, we obtain the system :

$$\left(\frac{\partial}{\partial t} + \boldsymbol{u}\cdot\nabla\right)\Phi_1 = \nabla\cdot(D\nabla\Phi_1) \tag{1a}$$

$$\left(\frac{\partial}{\partial t} + \boldsymbol{u}\cdot\nabla\right)\boldsymbol{u} = -\nabla p_0 + \frac{1}{\mathrm{Re}}\nabla\cdot(\nabla\boldsymbol{u} + \nabla\boldsymbol{u}^T) - \Phi_1\boldsymbol{e}_z \tag{1b}$$

$$\nabla\cdot\boldsymbol{u} = 0 \tag{1c}$$

which is non-dimensionalized by the velocity scale $U = \sqrt{\frac{(\varrho_1-\varrho_2)gL}{\varrho_2}}$, which is the free-fall, terminal velocity of the heavy fluid in the light one. The Reynolds number is defined as $\mathrm{Re} = \frac{\varrho_2 LU}{\mu_2}$. The characteristic length L is choosen as the length ℓ_0 of the heavy fluid volume initially released[1] (see Figure 1). All results are presented in this non-dimensional form, i.e. velocity is normalized by U, the distance $x*$ and cloud dimensions by L, and the time by $\frac{L}{U}$.

We use non-slip conditions on the boundary; the domain is chosen large enough so that its finiteness does not affect the solution.

[1] Note that often the characteristic lenght scale is taken as $L = \sqrt{\ell_0 h_0}$

Numerical method

Time discretization. In order to avoid the numerical instabilities that usually originate from half-implicit schemes with large time-steps, we use the characteristics method proposed by Pironneau (1989), i.e. we discretize directly the material derivative $\left(\frac{\partial}{\partial t} + \boldsymbol{u} \cdot \nabla\right)$ along the trajectory of a fictious particle $\boldsymbol{X}$ moving with the velocity $\boldsymbol{u}(\boldsymbol{X})$. It is thus possible to write an implicit Euler scheme for (1a) and (1b-1c).

Space discretization. We use the Taylor-Hood finite element (Taylor and Hood, 1973), that is a continuous piecewise quadratic approximation of $\boldsymbol{u}$ and Φ, and a continuous piecewise linear approximation of p. The equality (1c) is enforced up to machine precision by an augmented Lagrangian iterative algorithm (Fortin and Glowinski, 1983) over equations (1b-1c).

The flow being of "impulse" type, with locally high gradients in the shear and boundary layers, there is an obvious benefit in locally refining the mesh as shown in Figure 3 (Saramito and Roquet, 2000). We refine according to the Hessians of both the local energy dissipation and the phase volume-fraction in order to have the boundary layers and high-shear regions refined as well as the interface. It requires approximately 6 minutes to run a one-time-step iteration of 4 mesh adaptations on an Intel/Linux 1 GHz personal computer. A reasonable time-step is 0.05 in non-dimensional units, that is approximately 0.25 seconds for a large avalanche.

Results

Validation. Our validation in this article relies on the spatial growth and front velocity of the aerosol cloud as it moves down the slope. For a fine enough mesh, the features of the solution become mesh-invariant, which means that the numerical convergence is assured. It is shown in Figure 5 that the calculated front velocity is found similar to the experimental front velocity. In Figure 6 we compare the calculated evolution of cloud height and length with laws experimentally established by Beghin and others (1981) and by Rastello (2002). It is seen that the evolutions are similar.

Flow structure. As noted both in real avalanches and in laboratory clouds, the flow consists of two well identified parts, namely the head, which reaches large heights and develops shear-layer instabilities, and the tail (a wake), which is flowing more slowly, close to the ground. The numerical simulations display an even stronger separation between these two parts.

An essential feature is the ambient fluid entrainment, which causes the main drag. It is strongest at the rear of the head in experiments (Hopfinger and Tochon-Danguy, 1977; Rastello, 2002), and is also clearly so in our numerical simulations (Figure 2). The shear flow instability is also seen in the time sequence, Figure 4, and was found in both the above-cited experiments. Two other vortices rotating opposite to the shear-layer eddies are exhibited, one of them having been noticed by Rastello in experiments. Moreover, it was noted in these experiments that periodically, heavy fluid from the fore part of the head was rejected into the large vortex at the rear – a process also exhibited by the numerical simulations.

Kinetic energy and dynamic pressure. A well-known manifestation of avalanches is their destructive power, which is observed to be much larger in practice than estimated from the average density and front velocity (Berthet-Rambaud, 2001). One possible explanation is that the dynamic pressure inside the avalanche is locally much larger. The dynamic pressure is $\frac{1}{2}\varrho u^2$, and the ambient fluid density ϱ_2 being small in an avalanche, it is essentially equal to $\frac{1}{2}(\varrho_1 - \varrho_2)\Phi_1 u^2$. We compare it to the front average stagnation pressure, that is $\frac{1}{2}\bar{\varrho}u_f^2 \approx \frac{1}{2}(\varrho_1 - \varrho_2)\bar{\Phi}_1 u^2$, where $\bar{\varrho}$ (resp. $\bar{\Phi}_1$) is the average of the density (resp. of Φ_1) over the head. It is shown in Figure 7 that very high ratios are reached locally (around 7) where there are high velocities in dense areas. The existence of such large dynamic pressures inside the avalanche behind the front had been suggested by Hopfinger (1983) and was also noted by other authors (private communication from D. Issler, 2003).

Discussion

The direct numerical simulations presented in this article show that two-dimensional simulations reproduce the essential features of gravity currents, including avalanches. The assumption of two-dimensionality seems at first sight very stringent because the visual appearance of an avalanche flow in two-dimensions is quite different; the large vortices seen in avalanches as well as in laboratory clouds appear fully three-dimensional. Their strength, however, is determined by the two-dimensional mean shear, which justifies two-dimensional simulations as a good first approach. Indeed, the corresponding numercial results compare well with laboratory results. This is because the force balance is accounted for by the gravitational force which drives the avalanche, and entrainment of ambient fluid, which is the principal retarding force and is essentially a two-dimensional process. Since laboratory experiments with Boussinesq fluids are well reproduced in our simulations and since these laboratory avalanches have the same three-dimensional structures and involve the same governing mechanisms as the real avalanches, we can hope to simulate avalanches by taking into account the larger density difference. This requires the extension of the model and code to non-Boussinesq flows, which is currently in progress.

References

Beghin, P., E. J. Hopfinger and R. E. Britter, 1981. Gravitational convection from instantaneous sources on inclined boundaries. *J. Fluid Mech.*, **107**, 407–422.

Berthet-Rambaud, P., 2001. *Ouvrages en béton soumis aux avalanches: comparatif de deux outils de calculs*. Master's thesis, Université J. Fourier, Grenoble.

Dufour, F., U. Gruber and W. Ammann, 2001. Avalanches : études réalisées dans la Vallée de la Sionne en 1999. *Les Alpes*, **2**, 9–15.

Dufour, F., U. Gruber, P. Bartelt and W. Ammann, 2000. Overview of the 1999 measurements at the slf test site, vallée de la sionne. In *ISSW Conference Proceedings, A Merging of Theory and Practice*, 527–534.

Fortin, M. and R. Glowinski, 1983. *Augmented Lagrangian methods, applications to the numerical solution of boundary value problems*. Elsevier Science, Amsterdam.

Fukushima, Y. and G. Parker, 1990. Powder-snow avalanches: theory and application. *J. Glaciol.*, **36**(123), 229–237.

Hermann, F., J. Hermann and K. Hutter, 1987. Laboratory experiments on the dynamics of powder-snow avalanches. In Salm, B. and H. Grubler, eds., *Avalanches Formation, Movement and Effects (Proc. of the Davos Symposium, September 1986)*, 162, 431–440. IAHS Publ, Wallingford.

Hopfinger, E. J., 1983. Snow avalanche motion and related phenomena. *Ann. Rev. Fluid Mech.*, **15**, 47–76.

Hopfinger, E. J. and J.-C. Tochon-Danguy, 1977. A model study of powder-snow avalanches. *J. Glaciol.*, **19**(81), 343–356.

Hutter, K., 1996. Avalanche dynamics. In Singh, V. P., ed., *Hydrology of disasters*, 317–394. Kluwer Academic Publishers, Dordrecht etc.

Joseph, D. D. and Y. Y. Renardy, 1993. *Fundamentals of two-fluid dynamics*. Interdisciplinary Applied Mathematics. Springer Verlag, New-York, etc.

Naaim, M. and I. Gurer, 1998. Two-phase numerical model of powder avalanche, theory and application. *Natural Hazards*, **17**(2), 129–145.

Necker, F., C. Härtel, L. Kleiser and E. Meiburg, 2002. High-resolution simulations of particle-driven gravity currents. *Int. J. Multiphase Flow*, **28**(2), 279–300.

Normand, X., 1990. *Transition à la turbulence dans les écoulements cisaillés compressibles libres ou pariétaux*. Ph.D. thesis, Institut National Polytechnique de Grenoble, France.

Pironneau, O., 1989. *Finite Elements Methods for Fluids*. John Wiley & Sons, Chichester.

Rastello, M. C., 2002. *Étude de la dynamique des avalanches de neige en aérosol*. Ph.D. thesis, Université J. Fourier, Grenoble.

Rastello, M. C. and E. J. Hopfinger, in press. Sediment entraining suspension clouds : a model of powder-snow avalanches. *J. Fluid Mech.*.

Saramito, P. and N. Roquet, 2000. An adaptive finite elements method for viscoplastic fluid flows in pipes. *Comput. Methods Appl. Mech. Engrg.*, **190**, 5391–5412.

Taylor, C. and P. Hood, 1973. A numerical solution of the Navier-Stokes equations using the finite element technique. *Computers and Fluids*, **1**(1), 73–100.

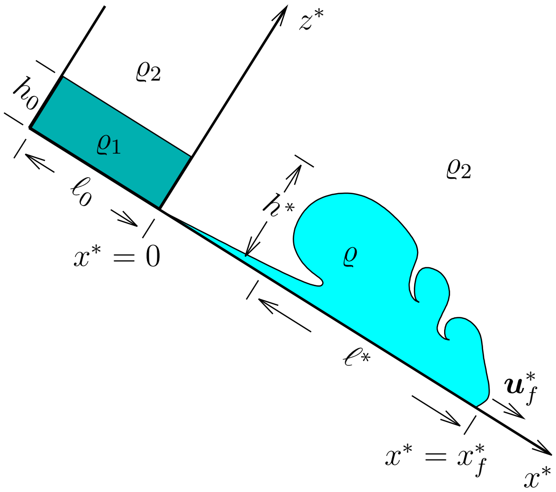

Figure 1: Definition sketch. The star denotes dimensional counterparts of quantities otherwise used in non-dimensional form.

2a. Laboratory cloud of Rastello (2002).

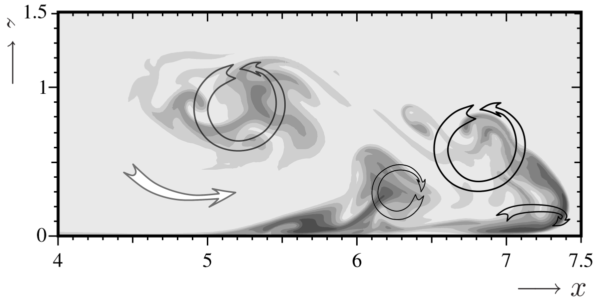

2b. Density map from numerical simulation.

Figure 2: Qualitative comparison between laboratory cloud and numerical simulation of a Boussinesq cloud at time $t = 12.8$ on a 32° slope, with $\mathrm{Re} = 10^4$. Superimposed in black are the large eddy motions and in white the air-entrainment process. The mesh of the front part is shown in Figure 3.

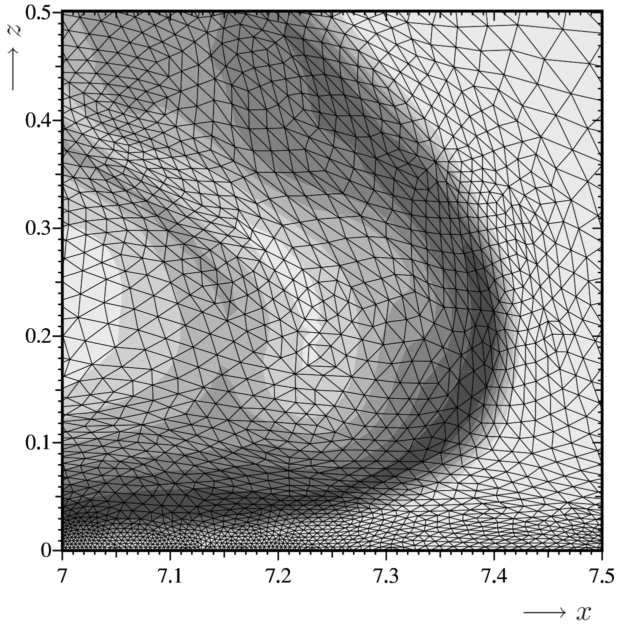

Figure 3: Detail of the adaptive mesh in Figure 2. Note the refinment in the boundary layer close to the ground and along the density map isolines (shown as background).

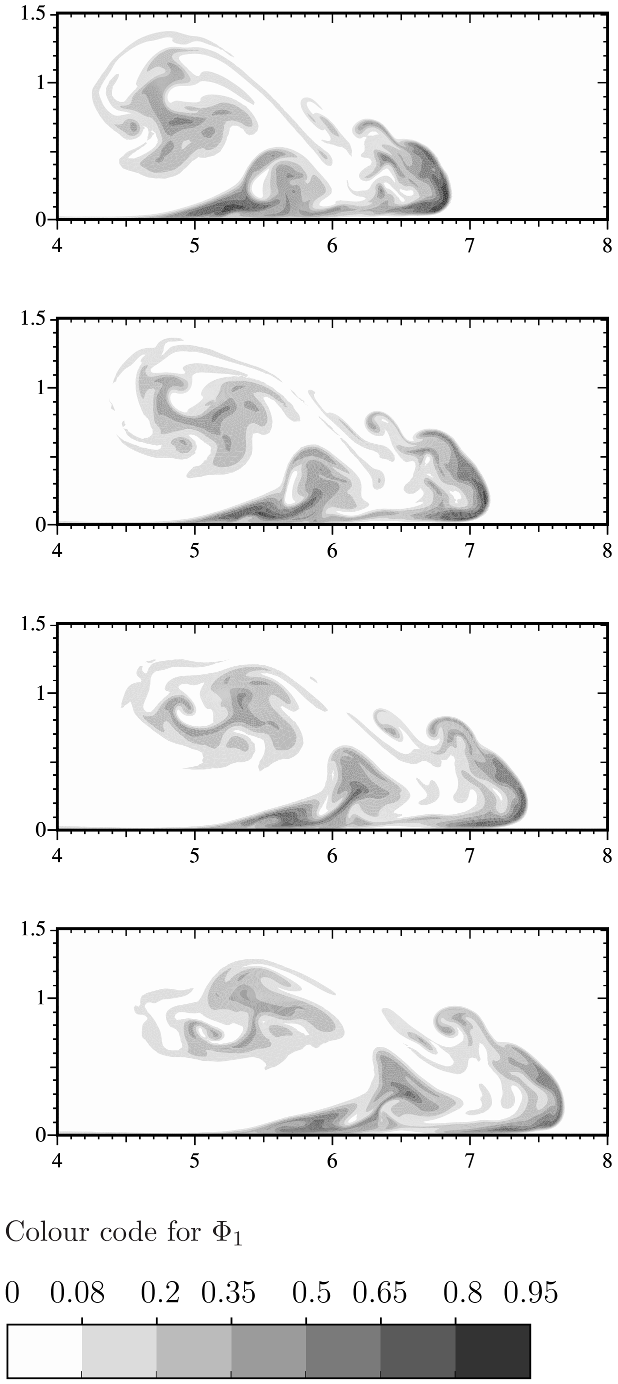

Figure 4: A time sequence of density maps in numerical simulations, for $t = 11.8$, $t = 12.3$, $t = 12.8$ and $t = 13.3$. Conditions are the same as in figure 2. Note that the maximum of Φ_1 diluted down from 1 to 0.95

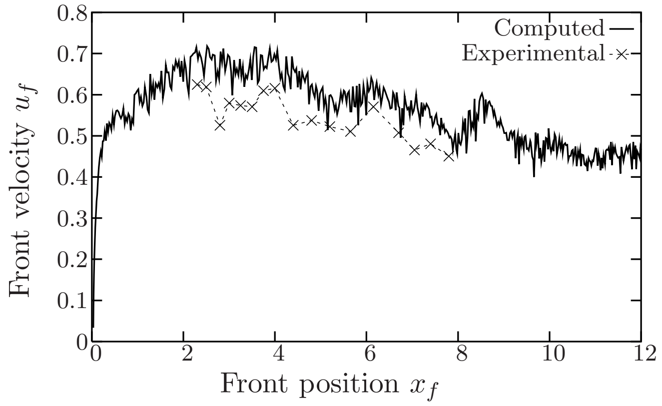

Figure 5: Comparison of the non-dimensional front velocity versus non-dimensional front position in simulations and in experimental clouds of Rastello (2002).

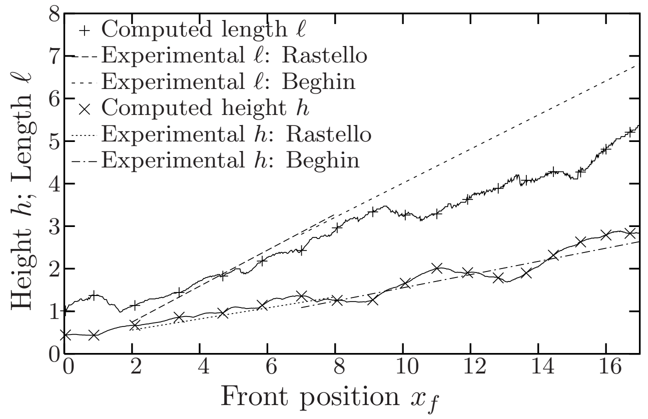

Figure 6: Comparison of the spatial growth of cloud length and height in simulations on a slope of angle $\theta = 32^o$ with the scaling laws from experimental clouds of Rastello (2002) and of Beghin and others (1981).

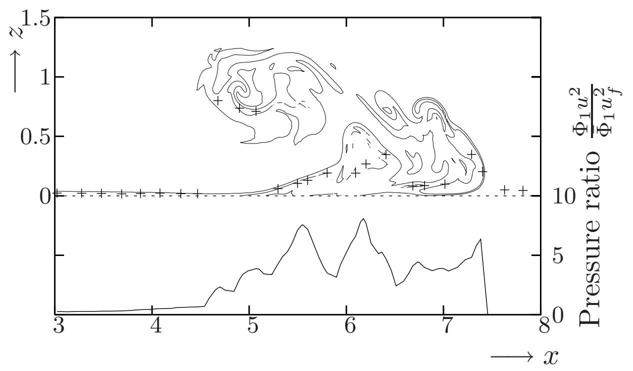

Figure 7: Ratio of maximum over z of excess dynamic pressure $\frac{1}{2}(\varrho_1 - \varrho_2)\Phi_1 u^2$ to front average stagnation pressure at $t = 12.8$. The '+' signs denote the loci of the maxima, isolines $\Phi = 0.08$ and $\Phi = 0.35$ are also shown.